

## Supplementary Material

# Siliceous subglacial deposits: archives of subglacial processes during the Last Glacial Maximum

Shalev Siman-Tov<sup>1</sup>, Terrence Blackburn<sup>2</sup>, Bernard Hallet<sup>3</sup>, Matthew A. Coble<sup>4,5</sup> and Emily E. Brodsky<sup>2</sup>

<sup>1</sup>*Geological Survey of Israel, 32 Yesha'ayahu Leibowitz, Jerusalem 9692100, Israel*

<sup>2</sup>*Department of Earth and Planetary Sciences, University of California, Santa Cruz, 1156 High Street., CA 95064, USA*

<sup>3</sup>*Quaternary Research Center, University of Washington, Seattle, WA, USA*

<sup>4</sup>*Stanford University, 367 Panama Street, Room 93, Stanford, CA, USA*

<sup>5</sup>*School of Geography, Environment and Earth Sciences, Victoria University of Wellington, Wellington, 6140, New Zealand*

**This file includes five supplemental figures, a table and text.**

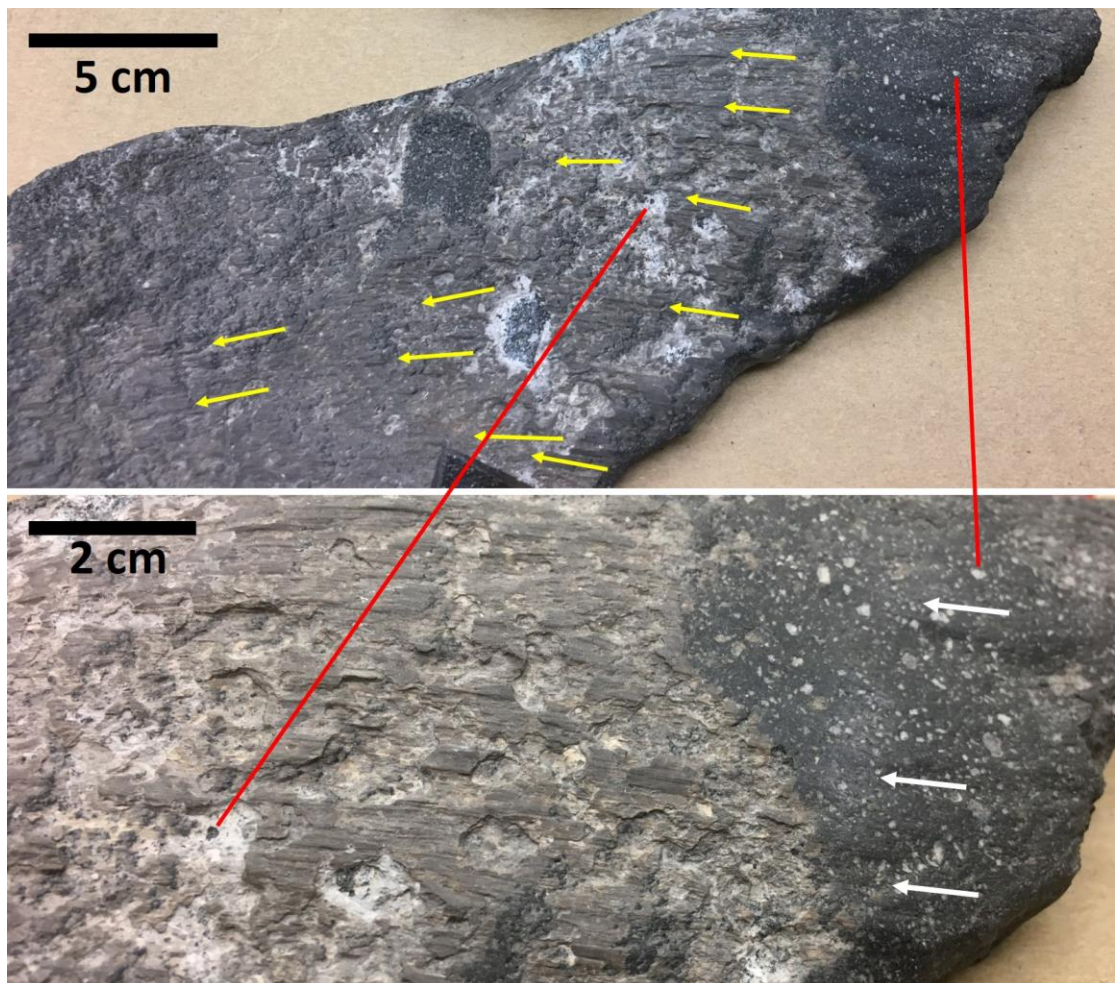


**Fig. S1.** Lineations in siliceous deposit and striations on bedrock trace the curving path of sliding ice, Mount Rainier, Washington, USA. Lineations (flutings) in the siliceous deposit are marked by yellow arrows in the upper, general view picture of the sample. Enlargement (red lines point on identical features on each photo) shows the closely parallel striations (white arrows) on stoss surface of glacially polished bedrock. It also shows the shallow pits in the deposit that reflect post-depositional weathering and erosion.

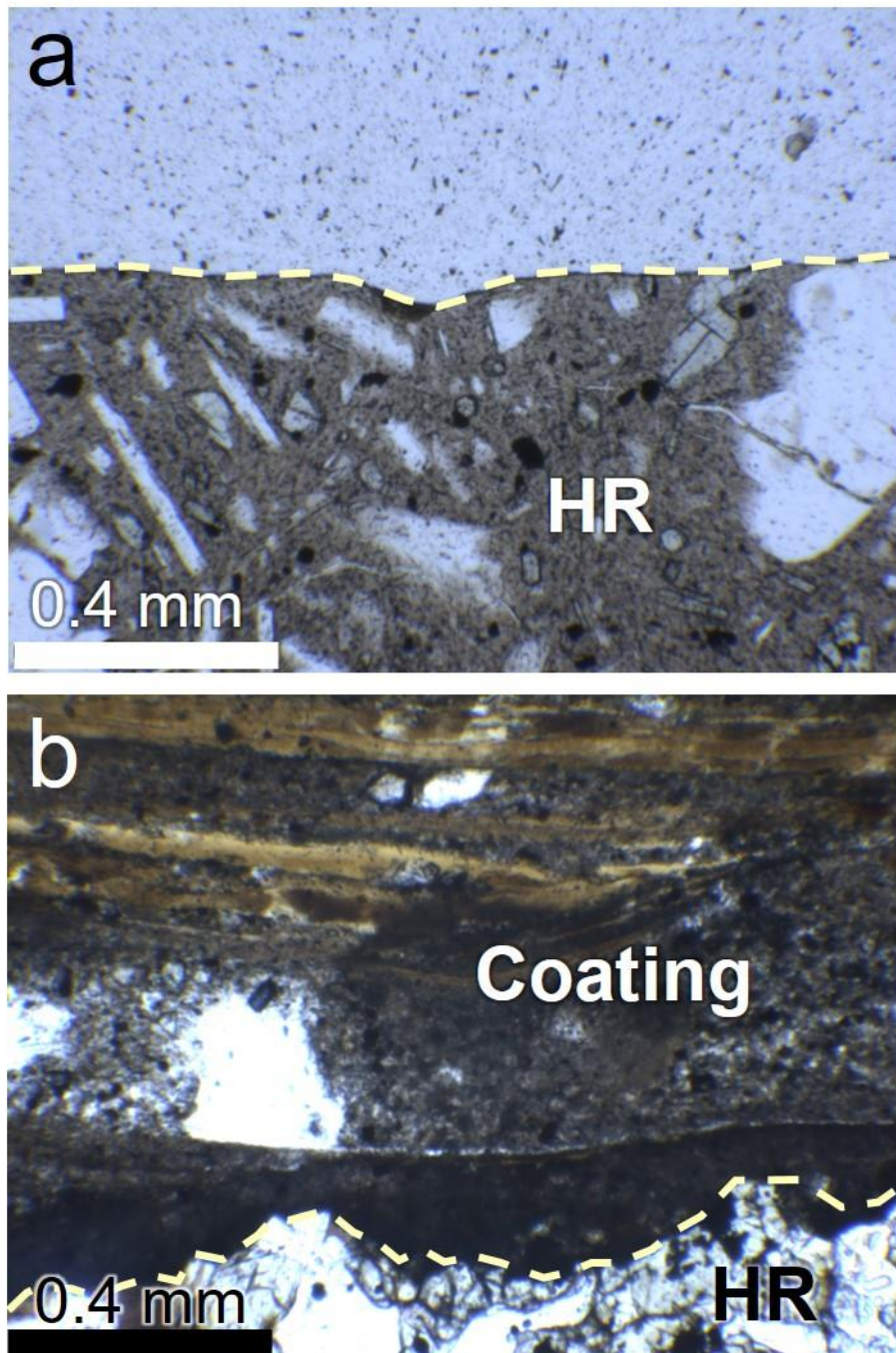


**Fig. S2.** Optical micrograph of thin sections cut in perpendicular to the host rock ('HR') surface. (a) Stoss side, cut transverse to the former sliding direction. (b) Lee side, cut parallel to the former sliding direction. The yellow dashed line marks the top of the bedrock.

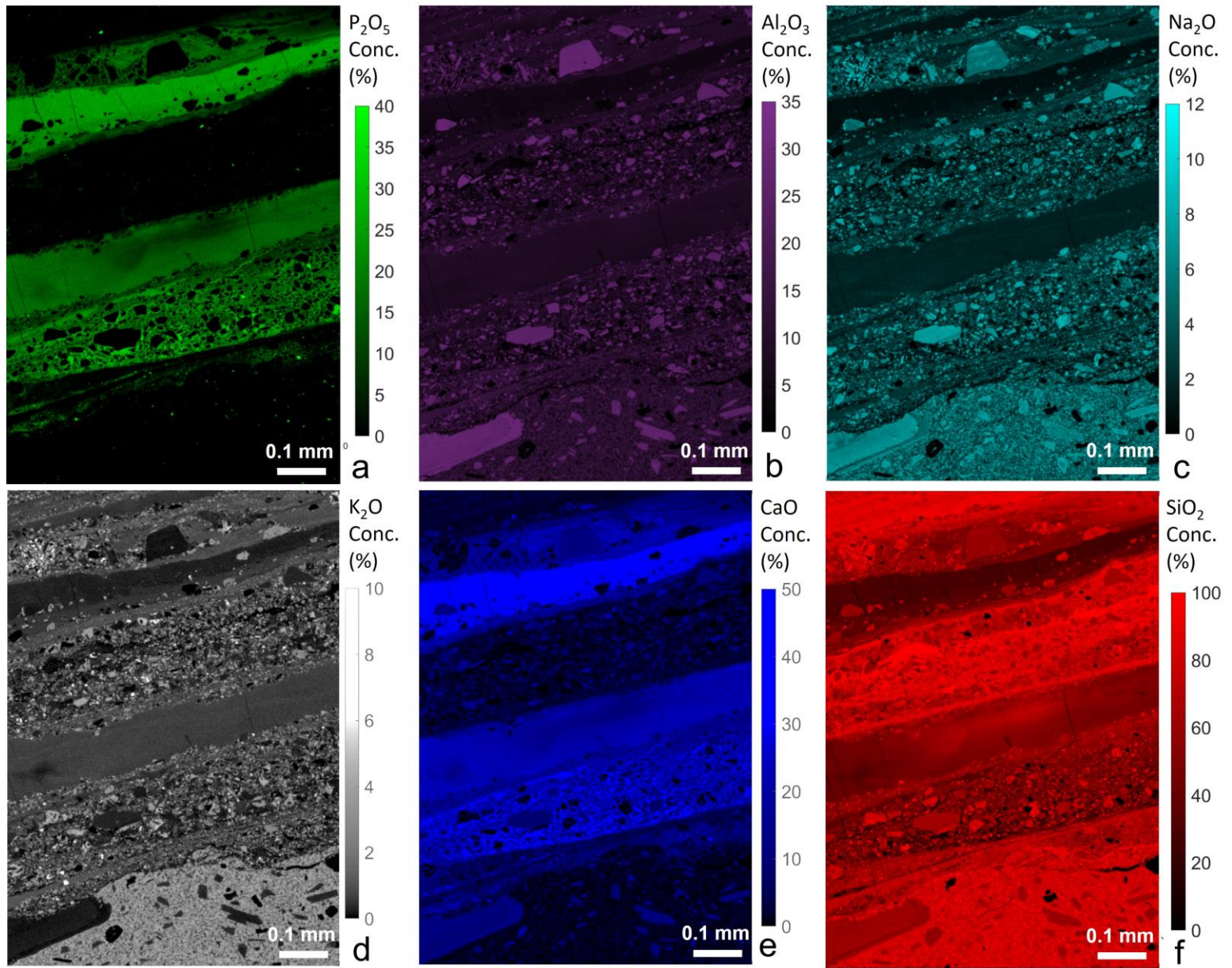


**Fig. S3.** Element maps, converted to oxides, are given for (a) P, (b) Al, (c) Na, (d) K, (e) Ca, (f) Si. The coating composition is clearly different from the andesite bedrock, suggesting that deposits are precipitated from subglacial solutions.

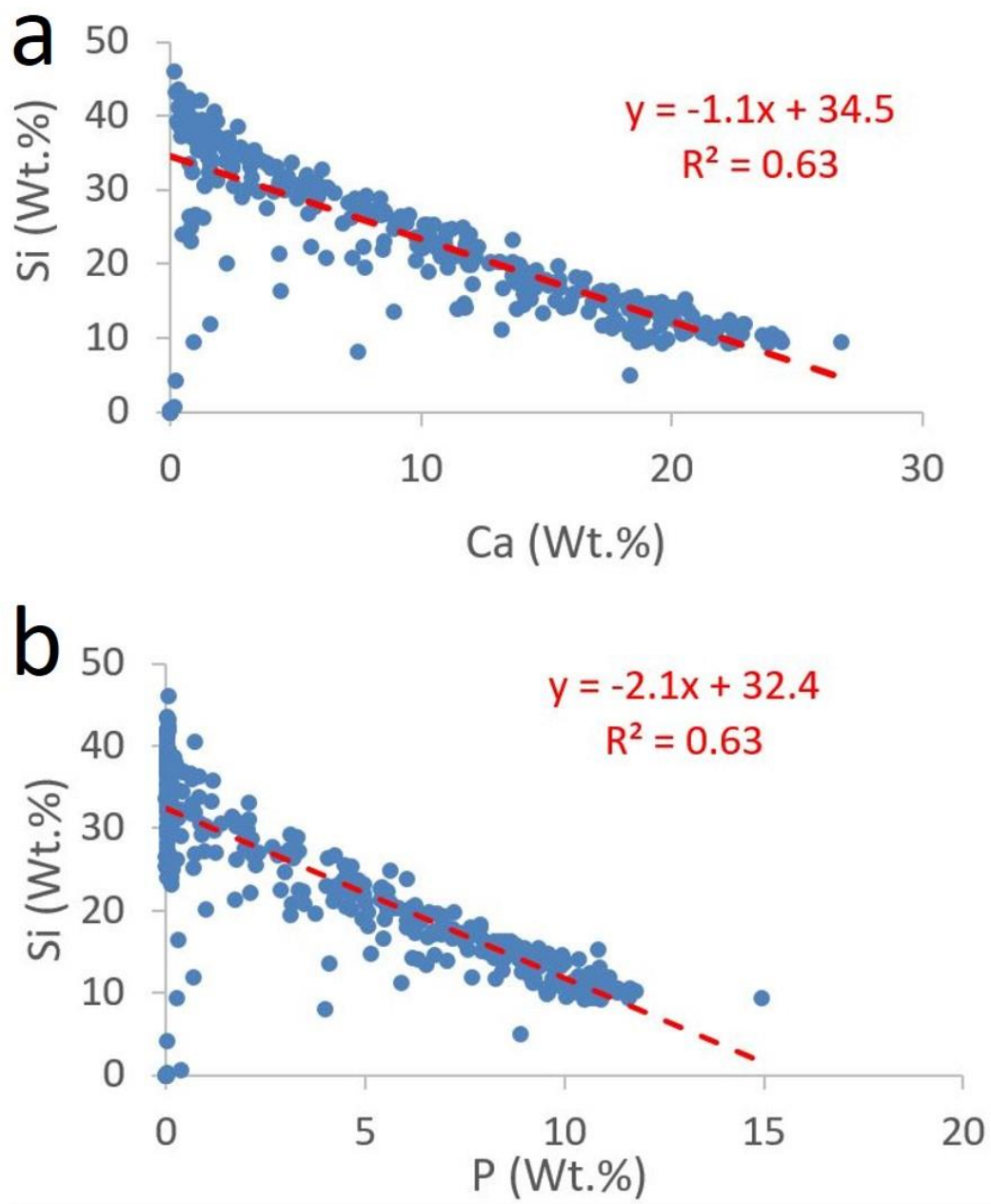


**Fig. S4.** Cross-plots of elemental concentrations measured in the siliceous deposit. The results of WDS line analysis in the EMPA suggest a negative correlation for (a) Si and Ca; and (b) Si and P. These results quantitatively show that the Si-rich layers are depleted in Ca and P, whereas the opposite is true for the Ca-rich layers (with high P and low Si).

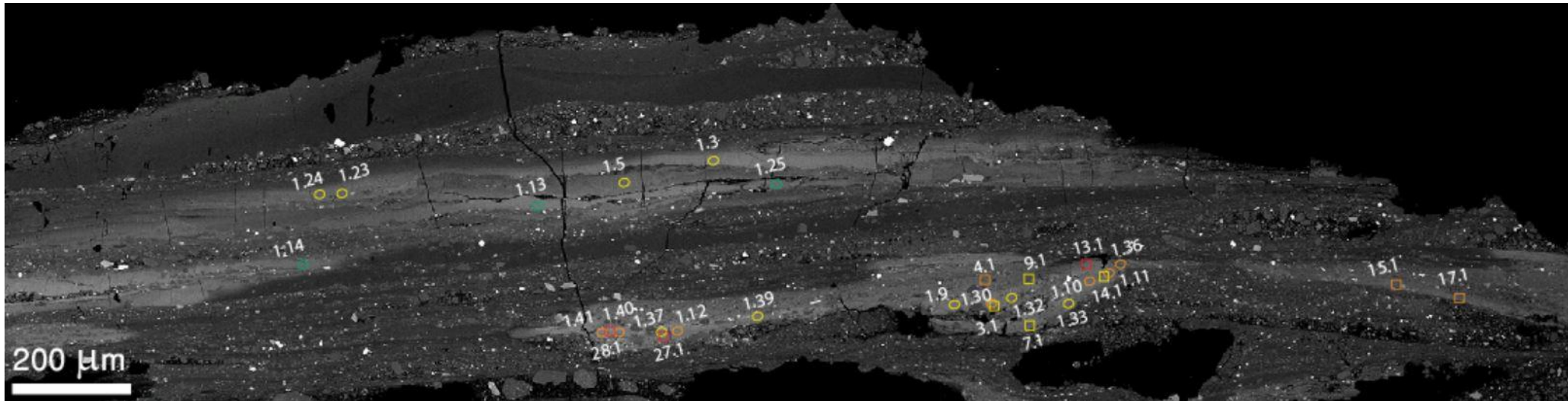


**Fig. S5.** Spot analysis locations on the backscatter electron (BSE) image of the siliceous deposits. The locations of the spot analyses for the first (ellipses) and second (squares) sessions (Table S1) are color coded according to their U content (in ppm): in green up to 5, >5 to 10 in yellow, >10 to 20 in orange and >20 by red. Only two layers have high enough U concentrations to yield statistically resolvable  $^{230}\text{Th}$  and  $^{234}\text{U}$  measurements. Uranium concentrations tended to be higher for the deepest siliceous layer.

Table S1. Detailed isotopic results. parentheses denote activity ratios.

**Session 1**  
**June 1-3, 2018**  
**Primary: O<sub>2</sub><sup>-</sup>**

Spot name	U/Si	$\pm 1\sigma$	( <sup>238</sup> U)/( <sup>232</sup> Th) <sup>a</sup>	$\pm 1\sigma$	( <sup>230</sup> Th)/( <sup>238</sup> U) <sup>a</sup>	$\pm 1\sigma$	corr ( <sup>238</sup> U)/( <sup>232</sup> Th) <sup>b</sup>	$\pm 1\sigma$	( <sup>230</sup> Th)/( <sup>232</sup> Th) <sup>a</sup>	$\pm 1\sigma$	corr ( <sup>230</sup> Th)/( <sup>238</sup> U) <sup>c</sup>	$\pm 1\sigma$	( <sup>234</sup> U)/( <sup>238</sup> U) <sup>a</sup>	$\pm 1\sigma$	U (ppm)	Th/U
Paradise-1.25	0.01493	0.0006	27.05	0.66	0.3442	0.13	26.67	0.66	9.25	3.39	0.349	0.135	3.552	0.324	2.9	0.12
Paradise-1.13	0.02444	0.0010	38.52	0.94	0.3077	0.15	37.98	0.94	12.60	6.66	0.312	0.151	2.303	0.162	4.8	0.083
Paradise-1.5	0.02812	0.0010	18.72	0.67	0.3049	0.09	18.46	0.67	5.21	2.16	0.309	0.094	4.854	0.436	5.6	0.17
Paradise-1.14	0.02547	0.0024	38.56	1.81	0.2218	0.09	38.02	1.81	9.25	3.61	0.225	0.090	2.592	0.158	5.0	0.082
Paradise-1.32	0.03022	0.0012	69.14	3.43	0.2699	0.05	68.17	3.43	18.65	3.55	0.274	0.056	2.045	0.217	6.0	0.046
Paradise-1.3	0.03195	0.0008	48.99	0.99	0.2662	0.07	48.30	0.99	13.56	3.80	0.270	0.077	2.161	0.136	6.3	0.065
Paradise-1.24	0.03437	0.0016	32.97	1.38	0.5473	0.15	32.51	1.38	16.72	4.84	0.555	0.149	2.824	0.229	6.8	0.096
Paradise-1.9	0.03489	0.0021	61.06	1.45	0.3266	0.08	60.21	1.45	20.28	4.84	0.331	0.087	2.218	0.170	6.9	0.052
Paradise-1.33	0.03527	0.0008	49.39	2.01	0.3335	0.06	48.69	2.01	16.99	3.06	0.338	0.069	1.953	0.163	7.0	0.064
Paradise-1.39	0.04123	0.0015	42.62	1.94	0.3195	0.07	42.02	1.94	13.58	2.85	0.324	0.073	2.721	0.119	8.1	0.075
Paradise-1.23	0.04022	0.0027	29.65	1.49	0.5136	0.26	29.23	1.49	18.76	7.67	0.521	0.257	3.200	0.146	7.9	0.107
Paradise-1.37	0.04842	0.0017	70.94	2.57	0.1934	0.07	69.94	2.57	14.50	4.46	0.196	0.073	2.206	0.095	9.6	0.045
Paradise-1.41	0.05216	0.0030	123.47	2.69	0.4124	0.10	121.74	2.69	53.87	10.98	0.418	0.101	1.434	0.111	10.3	0.026
Paradise-1.30	0.05510	0.0048	68.84	0.94	0.1627	0.06	67.87	0.94	11.94	4.00	0.165	0.062	1.968	0.102	10.9	0.046
Paradise-1.11	0.06112	0.0016	145.41	1.83	0.2351	0.04	143.37	1.83	34.90	5.36	0.238	0.046	1.754	0.073	12.1	0.022
Paradise-1.12	0.06794	0.0030	96.10	3.81	0.3131	0.12	94.75	3.81	33.96	14.04	0.318	0.124	1.842	0.083	13.4	0.033
Paradise-1.10	0.06628	0.0040	163.50	3.63	0.1817	0.06	161.21	3.63	30.21	12.82	0.184	0.066	1.241	0.073	13.1	0.019
Paradise-1.40	0.07621	0.0035	167.78	2.52	0.2267	0.06	165.42	2.52	41.31	10.49	0.230	0.064	1.691	0.064	15.0	0.019
Paradise-1.36	0.09223	0.0028	131.93	2.66	0.2254	0.03	130.08	2.66	29.95	3.42	0.229	0.038	1.611	0.054	18.2	0.024
BZVV-1.1	8.04	1.27	2945	265	0.982	0.020	2904	265	3038	367	0.996	0.033	1.015	0.033	1587	0.0011
BZVV-1.2	9.97	2.20	3401	678	1.004	0.017	3353.3	678.0	3834	943	1.019	0.031	1.016	0.023	1968	0.00094
BZVV-1.3	13.08	3.46	13575	2379	0.977	0.014	13384	2379.2	13643	2942	0.991	0.030	0.887	0.061	2583	0.00023
BZVV-2.1	7.87	1.85	6681	1456	0.963	0.018	6586.9	1456.3	6996	1347	0.977	0.032	1.009	0.017	1553	0.00048
BZVV-2.2	6.82	1.52	9131	2504	1.003	0.032	9003.0	2503.6	8426	2217	1.017	0.041	1.012	0.018	1346	0.00035
BZVV-2.3	7.18	1.66	10870	2288	0.963	0.020	10717	2288.4	9794	3541	0.977	0.033	0.919	0.016	1418	0.00029
BZVV-2.4	11.16	2.69	429399	176130	0.961	0.015	423371	176130	512578	198898	0.974	0.030	0.987	0.014	2203	0.000007
BZVV-2.5	6.85	1.78	5186	1552	1.035	0.037	5113.2	1552.3	5304	1748	1.049	0.045	1.022	0.016	1353	0.00061
611-1.1	1.68	0.31	3.0499	0.0034	0.0124	0.0078	3.007	0.026	0.083	0.040	0.013	0.027	23.43	0.19	461.5	1.04269
Average ( <sup>230</sup> Th/ <sup>238</sup> U) for BZVV:												0.986	0.026			

**Session 2**  
**July 11-12, 2018**  
**Primary: O<sub>2</sub>**

Spot name	U/Si	$\pm 1\sigma$	$(^{238}\text{U})/(^{232}\text{Th})^{\text{a}}$	$\pm 1\sigma$	$(^{230}\text{Th})/(^{238}\text{U})^{\text{a}}$	$\pm 1\sigma$	corr $(^{238}\text{U})/(^{232}\text{Th})^{\text{b}}$	$\pm 1\sigma$	$(^{230}\text{Th})/(^{232}\text{Th})^{\text{a}}$	$\pm 1\sigma$	corr $(^{230}\text{Th})/(^{238}\text{U})^{\text{c}}$	$\pm 1\sigma$	$(^{234}\text{U})/(^{238}\text{U})^{\text{a}}$	$\pm 1\sigma$	U (ppm)	Th/U	
Paradise-14.1	0.02562	0.0012	133.90	3.12	0.0889	0.05	129.08	3.12	11.62	6.59	0.092	0.065	1.618	0.094	5.7	0.024	
Paradise-7.1	0.02793	0.0010	32.35	3.48	0.2143	0.13	31.18	3.48	6.96	5.58	0.222	0.132	2.873	0.171	6.3	0.101	
Paradise-3.1	0.03526	0.0036	57.79	3.64	0.3128	0.08	55.71	3.64	19.66	4.93	0.324	0.092	1.874	0.135	7.9	0.056	
Paradise-9.1	0.03693	0.0013	62.00	1.93	0.1311	0.05	59.77	1.93	8.47	3.22	0.136	0.066	1.971	0.113	8.3	0.052	
Paradise-17.1	0.0477	0.0045	87.95	1.89	0.375	0.106	84.78	1.89	32.65	9.76	0.389	0.114	1.991	0.108	10.7	0.037	
Paradise-4.1	0.06379	0.0036	55.99	7.11	0.1535	0.05	53.98	7.11	9.32	3.58	0.159	0.062	2.099	0.171	14.3	0.058	
Paradise-15.1	0.0817	0.0091	56.19	2.22	0.305	0.077	54.16	2.22	15.90	3.71	0.316	0.087	2.045	0.101	18.3	0.058	
Paradise-13.1	0.12400	0.0104	32.48	3.46	0.0543	0.03	31.31	3.46	1.63	1.07	0.056	0.049	2.787	0.265	27.8	0.100	
Paradise-28.1	0.18615	0.0206	143.93	2.75	0.2940	0.12	138.75	2.75	49.55	10.47	0.305	0.127	1.401	0.089	41.7	0.023	
Paradise-27.1	0.23916	0.0414	106.31	9.27	0.1728	0.06	102.49	9.27	20.07	6.44	0.179	0.070	1.731	0.091	53.6	0.031	
BZVV-1.1	12.82	0.52	4306.3	561.1	0.9181	0.028	4151.2	561.1	3707.92	536.9	0.952	0.049	1.049	0.017	2870.9	0.00076	
BZVV-1.2	19.62	0.12	5351.0	1179.4	1.0142	0.020	5158.4	1179.4	4879.45	1123.6	1.052	0.045	1.030	0.026	4392.1	0.00061	
BZVV-1.3	18.30	0.69	19964.9	5417.9	0.9500	0.036	19246.1	5417.9	21336.42	9942.8	0.985	0.054	0.989	0.016	4098.6	0.00016	
BZVV-2.1	11.26	0.36	2002.6	357.5	0.9737	0.025	1930.5	357.5	2260.54	827.0	1.010	0.048	1.044	0.034	2520.3	0.0016	
NIST611-1.1	1.48730			3.058	0.0034	0.0240	0.023	2.948	0.041	0.07	0.1	0.025	0.047	20.652	0.153	462.5	1.06
NIST611-1.2	1.48063			3.051	0.0059	-0.0020	-0.012	2.941	0.041	-0.01	0.0	-0.002	0.042	20.329	0.152	460.5	1.07
Average (230Th/238U) for BZVV:												0.964	0.041				

<sup>a</sup> measured ratios

<sup>b</sup> measured  $(^{238}\text{U})/(^{232}\text{Th})^{\text{a}} * [\text{session average } (^{230}\text{Th})/(^{238}\text{U}) \text{ for BZVV}]$  to correct for mass discrimination

<sup>c</sup> measured  $(^{230}\text{Th})/(^{238}\text{U}) / [\text{session average } (^{230}\text{Th})/(^{238}\text{U}) \text{ for BZVV}]$  to correct for mass discrimination

## **SHRIMP-RG U-Th isotopic methods and data reduction**

U-Th isotopic measurements were performed using the SHRIMP-RG (sensitive high-resolution ion microprobe with reverse geometry) operated by Stanford University and the U.S. Geological Survey during two analytical sessions (Table S1): June 1<sup>st</sup>-3<sup>rd</sup>, 2018 and July 11<sup>th</sup>-12<sup>th</sup>, 2018. Analyses were performed on a polish rock sample that was cast in a 25 mm diameter epoxy disc alongside pre-polished reference materials (BZVV opal and NIST-SRM-611 glass. BZVV is a ca. 2.8 Ma porcelaneous biogenic opal (Virgin Valley, NV, USA; Paces and others, 2004; Amelin and Back, 2006) and is used here as a secular equilibrium reference material. The mounted samples were rinsed with a 10% EDTA solution (ethylenediaminetetraacetic acid) followed by distilled water and dried in a vacuum oven. The sample surface was coated with ~50 nm Au stored in a pre-evacuation chamber at ~10<sup>-7</sup> torr overnight prior to analysis to minimize degassing of the epoxy.

All analyses were performed by targeting the thickest amorphous polish that was free of mineral and/or rock fragments; guided by backscatter electron images (BSE) and reflected light images (Fig. S5). Individual analytical spots were measured using an O<sub>2</sub><sup>-</sup> primary ion beam focused to a spot size ranged from 35 to 45 microns in diameter, ~5-10 microns deep, and an intensity ranging from 7.8 to 9.3 nA. The acquisition routine included the following masses: <sup>28</sup>Si<sub>4</sub><sup>16</sup>O<sub>5</sub><sup>+</sup>, <sup>197</sup>Au<sup>+</sup>, <sup>238</sup>U<sup>+</sup>, <sup>232</sup>Th<sup>12</sup>C<sup>+</sup>, <sup>230</sup>Th<sup>16</sup>O<sup>+</sup>, background measured at 0.05 m/z above <sup>232</sup>Th<sup>16</sup>O<sup>+</sup>, <sup>234</sup>U<sup>16</sup>O<sup>+</sup> and <sup>238</sup>U<sup>16</sup>O<sup>+</sup>. All peaks were measured on a single ETP® discrete-dynode electron multiplier operated in pulse counting mode. Analyses were performed with 9-10 scans (peak-hopping cycles from mass 192 through 254) and count times for <sup>230</sup>Th<sup>16</sup>O<sup>+</sup> and <sup>234</sup>U<sup>16</sup>O<sup>+</sup> ranging from 90 to 120 seconds and 40 seconds, respectively. All measurements were performed at mass resolutions of M/ΔM = 7,000-8,500 (10% peak height) to avoid interfering isobaric interferences. The activity ratios (<sup>238</sup>U)/(<sup>232</sup>Th) were multiplied by the measured session average (<sup>230</sup>Th)/(<sup>238</sup>U) from BZVV to correct for mass discrimination.

Individual isotopic analyses were omitted if they contained low U (generally <5 ppm), <sup>230</sup>Th counts near background levels, or were in secular equilibrium (within 2 $\sigma$  analytical error). These omitted analyses are not reported in Table S1 and Fig. S5 because they either incorporated non-polish material and/or were inaccurate.

## **References cited**

- Amelin Y and Back M (2006) Opal as a U-Pb geochronometer: Search for a standard. *Chemical Geology* **232**(1–2), 67–86 (doi:10.1016/j.chemgeo.2006.02.018)
- Paces JB, Neymark LA, Wooden JL and Persing HM (2004) Improved spatial resolution for U-series dating of opal at Yucca Mountain, Nevada, USA, using ion-microprobe and microdigestion methods. *Geochimica et Cosmochimica Acta* **68**(7), 1591–1606 (doi:10.1016/j.gca.2003.08.022)